Available online at www.sciencedirect.com

ScienceDirect

International Journal of Solids and Structures 44 (2007) 2990–3003

INTERNATIONAL JOURNAL OF SOLIDS and STRUCTURES

www.elsevier.com/locate/ijsolstr

# Numerical simulations of 3D open cell structures – influence of structural irregularities on elasto-plasticity and deformation localization

Mathias H. Luxner [a,*], Juergen Stampfl [b], Heinz E. Pettermann [a]

[a] *Institute of Lightweight Design and Structural Biomechanics, Vienna University of Technology, Vienna, Austria*
[b] *Institute of Materials Science and Technology, Vienna University of Technology, Vienna, Austria*

Received 18 January 2006; received in revised form 30 August 2006
Available online 7 September 2006

**Abstract**

The mechanical properties of open cell structures made from an elastic–plastic bulk material are investigated by Finite Element simulations. The influence of structural irregularities on elasto-plasticity and deformation localization of open cell structures is analyzed. Six regular three-dimensional generic structures with a relative density of 12.5% are modeled by a unit cell approach for predicting the entire tensors of elasticity. From these six structures the two structures with the lowest and the highest elastic anisotropy are selected for further studies, introducing various degrees of structural irregularities. The effect of these irregularities on the linear and nonlinear behavior as well as the influence on the deformation localization is studied employing finite sample models. Results are presented by means of the direction dependent Young's moduli, deformation plots, overall stress–strain curves, and histograms of the energy distribution.


*Keywords:* Cellular structures; Structural irregularities; Disorder; Deformation localization; Elastic–plastic properties; Finite Element modeling

## 1. Introduction

Cellular materials are widespread in nature like in wood, in the interior of bone, and in many other living tissues. For engineering applications they gain increasing importance due to their low weight in combination with their particular properties. The mechanical behavior of cellular structures is governed by the internal architecture. In nature, the latter is adapted to the prevailing service conditions resulting in structures which are widely regarded as being optimized. Typically, nature produces irregular structures. The influence of these irregularities on the load bearing capacity, defect sensitivity, and robustness is not well understood at present.

* Corresponding author. Tel.: +43 1 58801 31721; fax: +43 1 58801 31799.
*E-mail address:* luxner@ilsb.tuwien.ac.at (M.H. Luxner).

0020-7683/$ - see front matter 
doi:10.1016/j.ijsolstr.2006.08.039

In the production of man-made cellular materials, e.g. by foaming of plastics and metals, it is quite difficult to control the internal structure and the arising irregularities strongly influence the overall mechanical behavior. Thus, the properties of such materials are not well reproduceable. The use of rapid prototyping techniques, however, opens the possibility of building structures with exact, predetermined geometries at high spatial resolution. Defined irregularities may be utilized to enhance the mechanical performance of such structures. Disorder can reduce the directional sensitivity of stiffness and strength, or can increase the energy absorption capabilities. Then, a sound understanding of the dependence of the properties of the cellular structure on their internal architecture becomes more important; in particular, knowledge on the influence of the irregularities is desired.

Therefore several analytical and numerical approaches can be found in the literature. Analytical models based on beam theory have been derived by Gibson and Ashby (1988) giving the effective mechanical properties as functions of the structures' relative density. Various analytical and numerical techniques considering the effective elastic behavior of low density regular cellular solids are presented by Grenestedt (1999) and Christensen (2000). Analytical methods (Zhu et al., 1997) and Finite Element simulations based on beam elements (Kwon et al., 2003) are used for analyzing the effective stiffness of open cell metallic foams with tetrakaidecahedral unit cells. In Gong and Kyriakides (2005) and Gong et al. (2005a,b) the linear and nonlinear compressive response of polyester urethane open cell foams is modeled using idealized periodic structures consisting of tetrakaidecahedral cells. Buckling and localization is considered and a comparison to experimental data is shown. Analytical and numerical analyses of the effective stress–strain behavior of a two-dimensional model foam in the nonlinear elastic regime are presented by Hohe and Becker (2003). Various three-dimensional open cell structures are studied in Luxner et al. (2004) and Luxner et al. (2005, 2006) using a periodic microfield approach. With respect to closed cell metallic foams a comprehensive treatise of simulation methods on both the micro and the macro scale can be found in Daxner et al. (1999, 2000), and Daxner (2003).

The influence of different kinds of structural imperfections on the effective mechanical properties of two- and three-dimensional cellular solids have been widely treated. Silva and Gibson (1997) investigate the effects of non-periodic microstructures and missing cell walls on elastic moduli, plastic collapse strength, and localization of deformation of two-dimensional cellular solids. In Guo and Gibson (1999) the localization behavior of two-dimensional honeycombs with and without defects is studied. Regular and irregular, low-density two-dimensional open-cell foams subjected to large deformations are investigated numerically by Shulmeister et al. (1998). Li et al. (2005) utilize the Voronoi tessellation technique and the Finite Element method to analyze the effect of irregular cell shapes and non-uniform cell wall thickness on the elastic properties of two-dimensional honeycombs. In the case of three-dimensional structures mostly Voronoi foams are utilized. Roberts and Garboczi (2002) investigate the elastic behavior of three-dimensional random foams. The effect of cell irregularity on the elastic properties of three-dimensional low-density open-cell Voronoi foams is analyzed by Zhu et al. (2000). Zhu and Windle (2002) model the high strain compression of low-density three-dimensional open-cell polymer foams. The mechanical behavior of linear elastic open cell foams is investigated by Gan et al. (2005) using three-dimensional Voronoi models.

The present study is concerned with modeling and simulation of the mechanical behavior of regular and irregular open cell low density porous structures by the Finite Element method. Mimicing cancellous bone, the influence of structural irregularities is investigated. Their effect on the linear and nonlinear mechanical behavior is evaluated under consideration of elastic–plastic bulk material properties, large strain theory, and deformation localization.

First, the linear elastic properties are investigated by a periodic microfield approach. Based on three-dimensional periodic unit cell models the entire elastic tensors are predicted for six different generic structures with perfect geometries. The anisotropic stiffness and the directional sensitivities are presented. Out of this six structures the two with the highest and the lowest degree of anisotropy are selected for further studies. On large periodic unit cells geometrical irregularities of varying magnitudes are introduced in the structures and their effect on the linear elastic behavior is studied.

Second, the nonlinear behavior is investigated in detail for the two selected structures, also taking into account deformation localization. Since the latter, in general, cannot be accomplished by means of periodic unit cell models, large finite samples are employed which are loaded by uniaxial compression. Different orientations of the structural lattice with respect to the loading direction are realized. As for the linear cases, perfect

structures are considered and a systematic study on the influences of structural irregularities is performed. On the one hand, the focus is set to the overall nonlinear response, in particular to the peak load and to the overall stress–strain behavior moderately beyond the load maximum. On the other hand, the influence of the geometric irregularities on the spatial deformation distribution is studied, i.e. whether or not deformation localization occurs and to which degree. In the present study a step by step approach is outlined for modeling the mechanical behavior of a class of complex structured porous materials.

## 2. Modeling approaches

Modeling of porous structures comprises two different tasks. First, the generation of particular geometries of the structures and, second, the set-up of appropriate representations within the framework of a computational method (here, the Finite Element Method). In the following the investigated structures and the computational modeling techniques are explained in detail.

### 2.1. Structural models

Six generic three-dimensional structures are selected attempting to choose various topologies with a variety of mechanisms governing their behavior. At first, all of them show regular geometries which are repeated periodically in all principal directions. The smallest periodic unit of a structure will be called 'base cell' in the present work. The six different base cells to be investigated are shown in Fig. 1 in the upper of each row. They comprise Simple Cubic (SC), Gibson Ashby (GA), Reinforced Body Centered Cubic (RBCC), and Body Centered Cubic (BCC) as already introduced in Luxner et al. (2005) as well as Kelvin (KV) and Weaire Phelan (WP) structures. Each structure exhibits a relative density of 12.5% and consists of struts with circular cross-sections with constant diameter. The dimensions of all base cells are $4\ \text{mm} \times 4\ \text{mm} \times 4\ \text{mm}$. All base cells possess cubic material symmetry. Note that only struts belonging to a single base cell are shown. This may appear incomplete at first sight, in periodic repetition, however, the structural geometries become obvious.

For periodic regular structures the consideration of a base cell is sufficient in most cases. When introducing structural irregularities, however, larger models are required. Irregular structures are generated for SC and KV topologies from arrangements of $8 \times 8 \times 8$ base cells. The vertices of the regular geometries are shifted to random positions by a fixed distance, $\delta$. For the shifting direction a spatially random distribution is adopted (Marsagli, 1972). The perturbation distance, $\delta$, is expressed in fractions of the strut length $l$ of the regular structure. Note that all struts of regular SC and KV structures exhibit equal length. Irregularities of $\delta/l = 1/16; 1/8; 1/4;$ and $3/8$ are realized, see Figs. 2 and 3 upper row. Such irregularities in the structures, however, increase the strut lengths and, consequently, effect the density. Thus, for representing the desired density the strut diameter is adopted accordingly.

Depending on the behavior to be predicted an appropriate modeling approach has to be selected. Accordingly, two different approaches for representing the structures as infinite and finite media, respectively, are employed. The first is achieved by using the periodic unit cell (periodic microfield) method (e.g. Anthoine, 1995; Pettermann and Suresh, 2000; Pahr, 2003; Böhm, 2004; Duschlbauer et al., 2006). The unit cell is the representation of a model material which is repeated periodically to fill infinite space. As such, opposing faces of the unit cell model must fit together. To achieve spatial periodicity of the deformation field appropriate coupling of the translational degrees of freedom of opposite unit cell boundary nodes is applied to the Finite Element model. In beam models, in addition, the rotational degrees of freedom of opposite unit cell boundary nodes need to be coupled. A set of masternodes is defined which carry the macroscopic translational deformations and the associated reaction forces. It is noted that the macroscopic rotational degrees of freedom are equal to zero within the framework of the periodic microfield approach. The masternodes allow for load application and response reading in terms of stresses and strains from which the entire elastic tensors can be computed. In this study models consisting of a single base cell are employed for the determination of the elasticity tensor of a perfect infinite structure. Unit cell models consisting of $8 \times 8 \times 8$ base cells with structural irregularities are used for the investigation of the influence of irregularities on the elastic behavior.

The periodic unit cell approach holds severe shortcomings in terms of deformation localization. Due to the strictly enforced periodicity, deformations cannot localize in arbitrary planes within the unit cell. To overcome

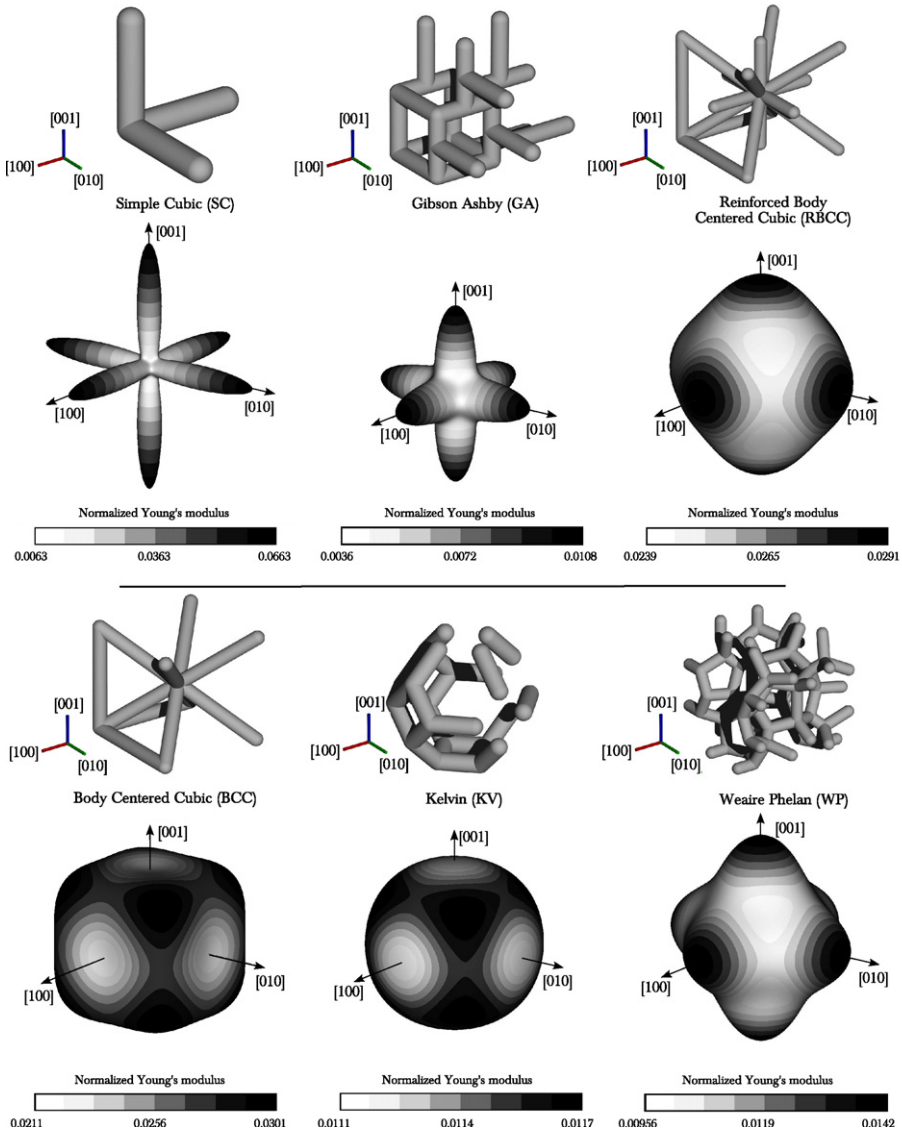


Fig. 1. Base cells of the investigated structures with a relative density of 12.5% (in the upper of each row) and their individually scaled normalized Young's moduli in all spatial directions (below); note the different scalings of the normalized Young's moduli.

the limits of the unit cell models, finite structures corresponding to test specimens (Luxner et al., 2004) are modeled in the second approach. Finite sample models are used for nonlinear investigations in which deformation localization can become an issue.

The uniaxial compressive response of cuboidal samples showing lattice orientations of [0 0 1], [0 2 1], [0 1 1], and [1 1 1] is investigated. The number of base cells is chosen to achieve sample dimensions of approximately 32 mm × 32 mm × 32 mm. The top face boundary conditions are taken to represent a rigid plate, which remains parallel to the (001) plane, otherwise it can move freely, and rotate around the [0 0 1] axis. This is achieved by coupling of the nodal displacements and rotations to the rigid body motion of a reference node using a feature of the FEM package ABAQUS/Standard (*Version 6.4.3*, *ABAQUS Inc.*, *Providence*, *RI*). Furthermore, all degrees of freedom of the bottom face nodes are locked, representing a rigid plate which is fixed. The finite sample analyses account for large deformations and elastic–plastic strut material.

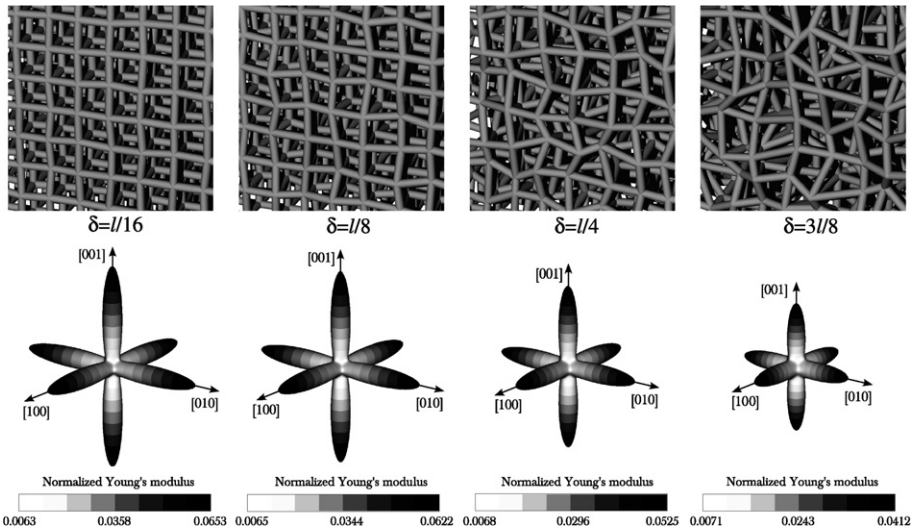


Fig. 2. Influence of structural irregularities, $\delta$, on the elastic behavior of the Simple Cubic structure; details of the irregular structures (top) and the predicted, equally scaled, normalized Young's moduli in all directions (bottom).

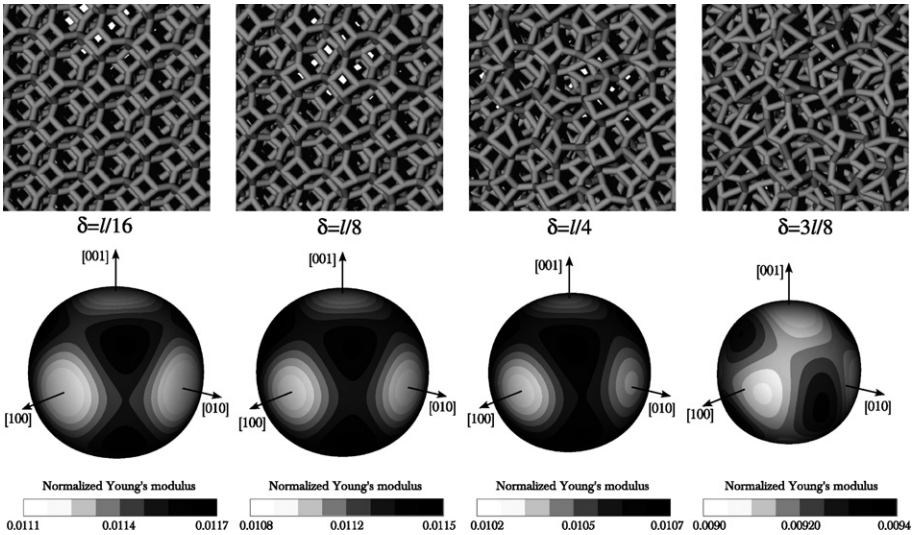


Fig. 3. Influence of structural irregularities, $\delta$, on the elastic behavior of the Kelvin structure; details from the irregular structures (top) and the predicted, equally scaled, normalized Young's moduli for all directions (bottom).

The present work is embedded in a larger program also including design, rapid prototyping, and experimental testing of open cell structures made from crosslinked photopolymers (Liska et al., 2003; Stampfl et al., 2004; Woesz et al., 2004) for which isotropic, elastic–plastic, strain rate independent material behavior is assumed. The Young's modulus of the bulk material, $E_s$, is 1700 MPa, the Poisson's ratio is 0.3. In Fig. 4 the uniaxial stress–strain curve of the bulk material is shown. $J_2$ plasticity and isotropic hardening are assumed.

### 2.2. Finite Element modeling

All numerical investigations are carried out by means of the Finite Element package ABAQUS/Standard. Beam element based models are utilized throughout this study. Straightforward beam modeling in the vicinity of the vertices would suffer from shortcomings; in general, the stiffness would be underestimated and the den-

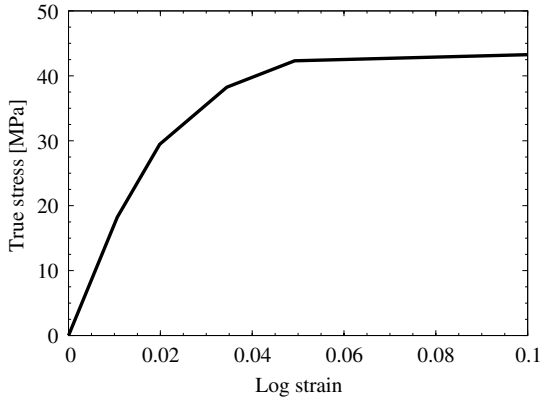


Fig. 4. Uniaxial stress–strain curve of the bulk material (crosslinked photopolymer); for strains larger than 0.1 linear extrapolation is used.

sity overestimated. Therefore, a spherical domain around each vertex is defined in which, first, quasi rigid beam elements are used and, second, the volume of the vertex region is represented by that spherical domain (and not by multiple overlapping beam elements). The radius of that sphere is set equal to the strut radius, which has to be determined to match the desired density of the model. Details of this modeling approach, verification, and comparison to continuum element models are given in Luxner et al. (2005) and Luxner (2006).

Timoshenko beam elements with three nodes and quadratic interpolation functions are used to allow for bending and transverse shear deformations. At least four elements are used for discretization of the deformable part of a single strut. For the beam cross sections the number of Gauss points is chosen to be 24 (eight in circumferential direction times three in radial direction). No contact or self contact is considered.

When bifurcation or buckling can become an issue, care has to be taken not to proceed along the trivial equilibrium path. For the perfect SC structure loaded in the principal direction a small transverse force is applied to induce buckling affine deformations. For all other cases belonging to the SC set, localization (if existing) starts from the boundary of the sample or is triggered by structural irregularities. For the KV structures the Gauss points in various beam elements are oriented unevenly which is sufficient to act as (numerical) imperfections. In general, instability problems of the present kind involving elastic–plastic materials are highly complex and not within the scope of the present work.

## 3. Results and discussion

### 3.1. Elastic anisotropy

First, the anisotropy of the linear elastic stiffness of the regular structures is investigated for all six cases. Periodic unit cell models of single base cells are employed and the required number of independent load cases is solved for each structure. From these responses the entire elastic tensors are assembled, see Pahr (2003) and Duschlbauer et al. (2006). The Young's moduli in all spatial directions are extracted by rotational transformations of the tensors. In Luxner et al. (2005) the Young's moduli, $E^*$, (normalized by the Young's modulus of the bulk material, $E_s$) of SC, GA, RBCC, and BCC for directions within the (1 0 0) and $(1\bar{1}0)$ planes are presented in polar plots. Here, three-dimensional visualizations of the normalized Young's moduli of these structures are given in Fig. 1. Additionally, the normalized Young's moduli of the KV and the WP structures with the same relative densities are shown. Note that for better visualization the scale of the normalized Young's moduli's contours is different for different structures. The normalized Young's moduli for the orientations [0 0 1], [0 2 1], [0 1 1], and [1 1 1] are listed in Table 1. Since all structures show cubic material symmetry, the extremal stiffness values appear in the [0 0 1] and the [1 1 1] direction (Nye, 1985). The SC structure shows the most pronounced anisotropy and directional sensitivity with respect to the Young's modulus. It exhibits very stiff behavior in the principal directions and shows a strong decrease of the stiffness apart the principal directions. In contrast, the KV structure is the most isotropic one which exhibits nearly equal values for the

Table 1
Predicted normalized Young's moduli, $E^*/E_s$, of the perfect Simple Cubic (SC), Gibson Ashby (GA), Reinforced Body Centered Cubic (RBCC), Body Centered Cubic (BCC), Kelvin (KV), and Weaire Phelan (WP) structures for a relative density of 12.5% at selected directions

| | $E^*/E_s \times 10^{-2}$ | | | |
|---|---|---|---|---|
| | [001] | [021] | [011] | [111] |
| SC | 6.630 | 1.193 | 0.816 | 0.631 |
| GA | 1.080 | 0.551 | 0.432 | 0.360 |
| RBCC | 2.906 | 2.632 | 2.499 | 2.389 |
| BCC | 2.106 | 2.460 | 2.716 | 3.007 |
| KV | 1.109 | 1.140 | 1.158 | 1.174 |
| WP | 1.421 | 1.152 | 1.041 | 0.956 |

normalized Young's modulus in all directions. The maximum occurs for the [1 1 1] direction. Because of the significant difference in their anisotropy, SC and KV are chosen for subsequent investigations.

Next, the influence of structural irregularities on the elastic behavior of the SC and the KV structures is investigated. Because of the random character of the irregularities single base cells are no longer sufficient. Still, unit cell models are employed but consist now of some $8 \times 8 \times 8$ base cells. For easier application of periodic boundary conditions the vertices located at the unit cell boundaries remain unchanged. Inside the cells structural irregularities are introduced as described in Section 2.1. Four different degrees of perturbation are analyzed. For each of them five different models are generated (having the same statistical descriptors but different discrete realizations) and the elastic tensors are predicted. Figs. 2 and 3 show details from the irregular structures (top) and the normalized Young's moduli for all directions (bottom). The latter show one out of the five corresponding models for each perturbation. The contour scaling is individual for each plot and the length scaling is the same for all plots in a figure. More details on the statistical variation of these results are given in Table 2, which lists the average, minimum, and maximum values of the normalized

Table 2
Minimum, maximum, and average values of the predicted normalized Young's moduli, $E^*/E_s$, of Simple Cubic and Kelvin structures with various irregularities, $\delta$, for a relative density of 12.5% at selected directions; for each irregularity five models are analyzed

| | | $E^*/E_s \times 10^{-2}$ | | | | | |
|---|---|---|---|---|---|---|---|
| | | Simple Cubic | | | Kelvin | | |
| | | Min. | Max. | Avg. | Min. | Max. | Avg. |
| [001] | $\delta = 0$ (perfect) | – | – | 6.630 | – | – | 1.109 |
| | $\delta = l/16$ | 6.516 | 6.528 | 6.524 | 1.100 | 1.104 | 1.103 |
| | $\delta = l/8$ | 6.192 | 6.242 | 6.219 | 1.081 | 1.085 | 1.083 |
| | $\delta = l/4$ | 5.178 | 5.260 | 5.211 | 1.011 | 1.035 | 1.024 |
| | $\delta = 3l/8$ | 4.072 | 4.151 | 4.103 | 0.894 | 0.912 | 0.905 |
| [021] | $\delta = 0$ (perfect) | – | – | 1.193 | – | – | 1.140 |
| | $\delta = l/16$ | 1.197 | 1.199 | 1.198 | 1.132 | 1.135 | 1.134 |
| | $\delta = l/8$ | 1.207 | 1.213 | 1.210 | 1.111 | 1.115 | 1.113 |
| | $\delta = l/4$ | 1.242 | 1.268 | 1.249 | 1.038 | 1.046 | 1.044 |
| | $\delta = 3l/8$ | 1.174 | 1.304 | 1.238 | 0.911 | 0.929 | 0.918 |
| [011] | $\delta = 0$ (perfect) | – | – | 0.816 | – | – | 1.158 |
| | $\delta = l/16$ | 0.820 | 0.821 | 0.820 | 1.149 | 1.152 | 1.150 |
| | $\delta = l/8$ | 0.831 | 0.834 | 0.833 | 1.125 | 1.131 | 1.128 |
| | $\delta = l/4$ | 0.867 | 0.889 | 0.875 | 1.053 | 1.059 | 1.056 |
| | $\delta = 3l/8$ | 0.843 | 0.940 | 0.891 | 0.914 | 0.932 | 0.923 |
| [111] | $\delta = 0$ (perfect) | – | – | 0.631 | – | – | 1.174 |
| | $\delta = l/16$ | 0.634 | 0.636 | 0.635 | 1.165 | 1.169 | 1.167 |
| | $\delta = l/8$ | 0.644 | 0.647 | 0.645 | 1.138 | 1.145 | 1.142 |
| | $\delta = l/4$ | 0.671 | 0.681 | 0.680 | 1.056 | 1.068 | 1.065 |
| | $\delta = 3l/8$ | 0.700 | 0.715 | 0.708 | 0.913 | 0.950 | 0.928 |

Young's moduli evaluated from the corresponding five models. The directions referred to always pertain to the regular structures from which the irregular geometries are derived.

In the case of the SC structure it can be seen that with increasing perturbation magnitude the normalized Young's moduli in the principal directions decrease, whereas for the other directions the normalized Young's moduli increase. A pronounced anisotropy remains even for the most irregular case. The directions of the extremal values are unchanged compared to the regular structure.

The KV structure shows a decrease of the normalized Young's moduli for all directions. Note that for the most irregular case the Young's moduli are nearly uniform with respect to the direction, and that the extremal values are no longer aligned with the principal directions of the regular structure. Zhu et al. (2000) give predictions for foams with markedly lower densities where irregularities cause stiffening.

### 3.2. Nonlinear behavior – deformation localization

So far the linear elastic behavior was considered for which periodic unit cells (of different sizes) are appropriate tools. They can also handle nonlinear deformations to a certain extent, however, other approaches have to be adopted for modeling deformation localization. The latter, here, is defined by the existence of a region which spans a wide area in a structure in two dimensions, and has a rather limited extension in the third direction. This region is not necessarily plane. Note that localization is always accompanied by a small region of high strains and a large region of considerably lower strains. In contrast, stress drops with evenly distributed strains all over the structure are rather considered as "softening". The following investigations are based on finite samples which are loaded by uniaxial compression.

Again, the SC and the KV structures are studied. The results are given in terms of selected plots of deformed structures, overall stress–strain curves, and histograms showing the total energy distribution in the models. The results as being presented are restricted to the deformation domain before the onset of contact.

#### 3.2.1. Perfect geometries

In Fig. 5 (first column) the deformation patterns of the perfect SC structures at four different lattice orientations are shown without scaling the deformations. Pronounced localization of deformation can be seen. For the load cases [0 0 1] and [0 2 1] the localization takes place in a principal structure plane extending over one and two layers, respectively. The latter described deformation, however, is only one feature of the localization. The second information for fully describing the localization is the component of displacement within that plane, i.e. the direction in which the struts tilt, and will be called localization displacement. For the load cases [0 0 1] and [0 2 1] the localization displacements occur along a principal structure direction. In the [0 1 1] orientation the localization takes place in two perpendicular planes forming an '*X*', also showing localization displacements in principal directions. Note that, here, localization is triggered at the edge where the free and the fixed faces meet, and other sample sizes are expected to give rise to different deformation patterns. For the perfect [1 1 1] case no distinct localization can be seen. The deformation concentrates in (0 1 1) planes but extends over the entire region which is not affected by the top and bottom constraints.

The overall stress–strain curves corresponding to the above scenarios are shown in Fig. 6 by solid lines. In all cases plastic yielding starts well before deformation localization sets on. For [0 0 1] compression the highest peak load is reached at the smallest overall strain followed by a sharp drop upon localization. In [0 2 1] and [0 1 1] loading the behavior is quite similar with markedly reduced peak values at higher overall strains and only a moderate load reduction upon localization. Finally, the [1 1 1] case shows the lowest peak load almost without a subsequent decrease at high overall strains.

The behavior of the perfect KV structures for the selected orientations is given in Fig. 7 by the solid lines. All predictions are very similar both with respect to the peak loads and the corresponding overall strains as well as with respect to the rather smooth shapes of the curves. Similar to the elastic behavior, the directional strength dependence is rather insignificant for the KV structures. The minimum peak value is predicted for the [1 1 1] orientation, the maximum for the [0 1 1] orientation. Note that this is in contrast to the present elastic predictions, where [1 1 1] yields the highest Young's modulus and [0 1 1] has an intermediate value.

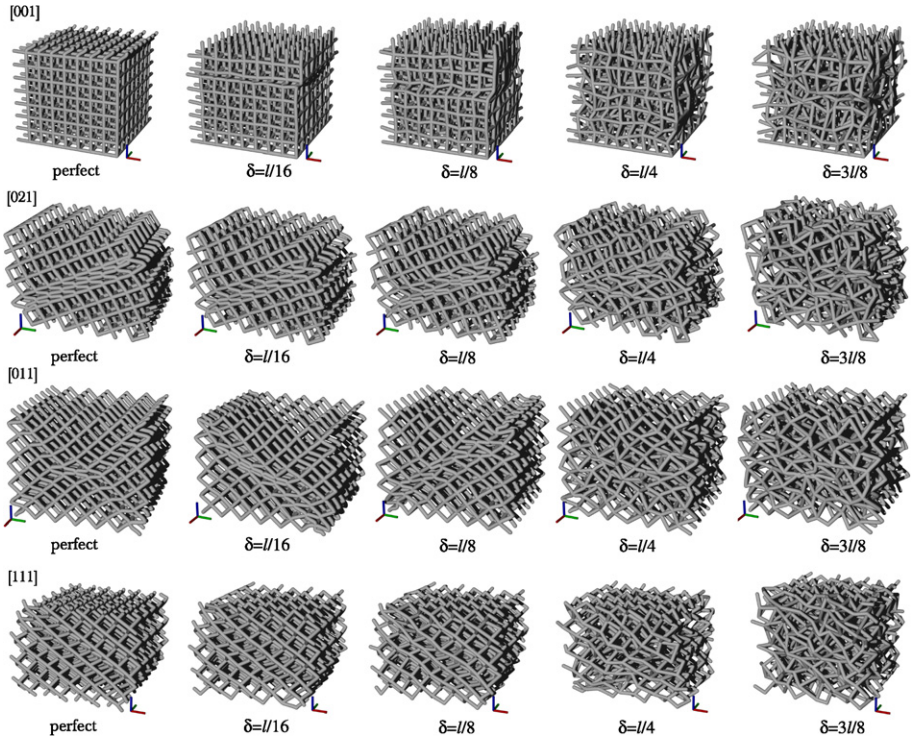


Fig. 5. Predicted deformation patterns of Simple Cubic finite structures under uniaxial vertical compression for increasing perturbation size, $\delta$, (from left to right) and for lattice orientations [0 0 1], [0 2 1], [0 1 1], and [1 1 1] (from top to bottom); the displacement scale is 1.

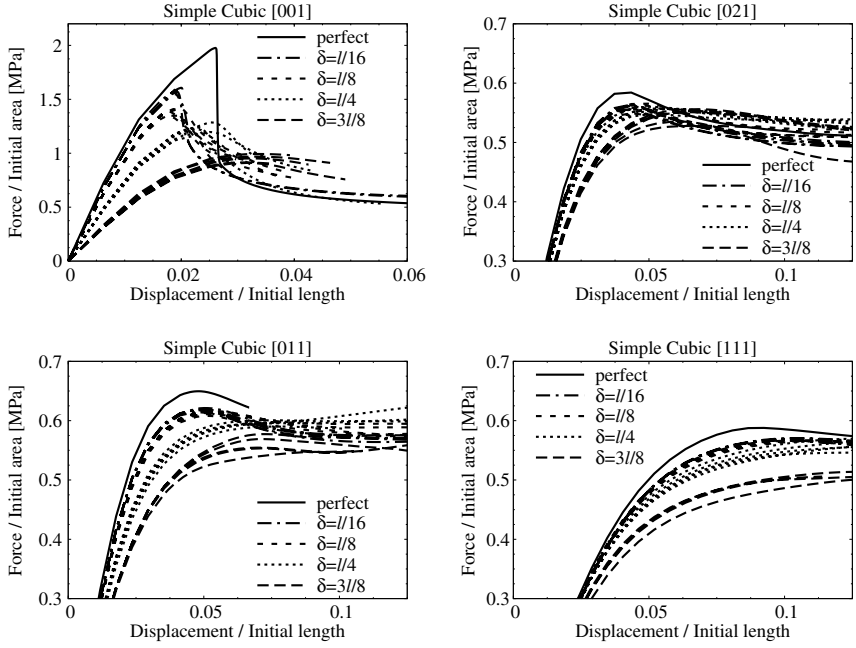


Fig. 6. Predicted overall stress–strain curves of Simple Cubic finite structures with different irregularities, $\delta$, for lattice orientations [0 0 1], [0 2 1], [0 1 1], and [1 1 1] with respect to uniaxial compression.

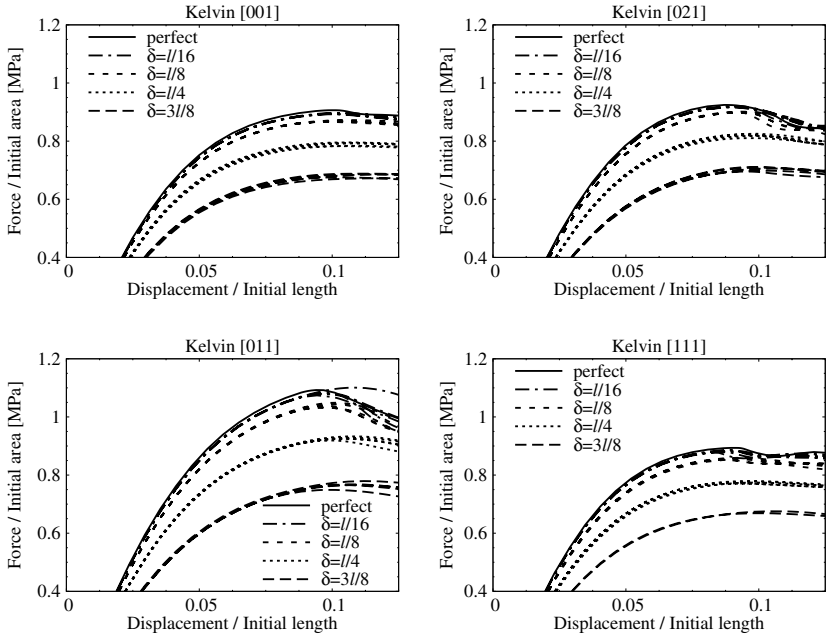


Fig. 7. Predicted overall stress–strain curves of Kelvin finite structures with different irregularities, $\delta$, for lattice orientations [0 0 1], [0 2 1], [0 1 1], and [1 1 1] with respect to uniaxial compression.

From the deformed structures (not shown) no localization is obvious. For all cases the distributions of the deformations are rather homogeneous over the height of the samples. Note that a decreasing overall stress at higher overall strains is not a sufficient criterion for the occurrence of localization.

### 3.2.2. *Influence of structural irregularities*

In this section the influence of structural irregularities on the global stress–strain behavior and on the deformation localization is investigated. Again, five models for each perturbation magnitude are generated and analyzed. Analyses are performed for lattice orientations of [0 0 1], [0 2 1], [0 1 1], and [1 1 1].

Fig. 5 shows the predicted deformations of the SC models with structural irregularities of different degree (together with the regular structures) under uniaxial compression for the selected orientations. For small irregularities the behavior is similar to the perfect structures and the deformation localizations occur in the same manner. With increasing irregularities the localizations are less obvious and at pronounced irregularities no localization can be seen in the deformed structures of all orientations.

Fig. 6 shows the corresponding stress–strain curves for these cases. The predictions of all five realizations of each single case are shown. Inspection of the [0 0 1] orientation reveals, at first, the previous result that for increasing perturbation the stiffness of the structures decreases. With increasing deviation of the vertices from their location in the regular structure the governing deformation mechanism changes from pure axial compression in the struts to a mixed mode with increasing bending contribution. The peak load is reduced and shifted to higher strains for increased irregularities. Also the load drop following the maximum load is less pronounced, resulting in a higher load carrying capacity at larger displacements. For the [0 2 1], [0 1 1], and [1 1 1] orientations the same trends can be seen, but much less pronounced. The structures tend to exhibit more compliant behavior and lower strength with increasing perturbation size, and the load drop after the peak is less pronounced. Note that the linear elastic behavior as discussed earlier, here, is superimposed by free surface effects, the chosen boundary conditions, and the nonlinear behavior of the bulk material, see Luxner et al. (2006).

For the KV structures the predicted overall stress–strain diagrams for various irregularities are given in Fig. 7. For all orientations the irregularities show a moderate decrease of the peak loads. The qualitative behavior is not effected by irregularities. These results support the finding from Section 3.2.1 that KV structures are not susceptible to deformation localization.

### 3.3. Influence of relative density

The present study is carried out under the premise of a single relative density which is kept constant for all investigations. Since the introduction of irregularities gives rise to longer struts in average, their diameters have to be adjusted accordingly to keep the relative density constant. The effect when keeping the struts' diameter constant is discussed for the following example. The SC structure with a perturbation of magnitude $\delta = 3l/8$ and no diameter correction increases its relative density from 12.5% to 13.8%. For the case of the [0 0 1] orientation without diameter correction the predicted peak load is 22% higher than for the structure with diameter correction.

### 3.4. Spatial energy distribution

Spatially localized concentrations of deformations have been shown in Fig. 5. The evaluation of such figures is rather intuitive. For pronounced localization the effect is quite obvious, for the cases of increasing perturbation, however, assessment of the deformed structures becomes more difficult.

Considerations of the total (spatial) energy distribution in the structures can be helpful in evaluating the localization of deformations. The characteristics of this localization area is, that the major part of the (overall) deformation is concentrated in it, and that the stresses with respect to the corresponding planes are (rather) continuous. This means, as a direct consequence, the energy of overall deformation is predominantly concentrated in this areas.

This effect is visualized in terms of energy histograms. For that purpose the total energy in each beam element normalized by the total overall energy is plotted vs. the relative occurrence. The latter is the number of elements sharing energy values within the same interval divided by the total number of elements. As third axis the overall displacement is used. This way, excessive energy consumption of a certain fraction of beam elements, i.e. localization, can be detected.

For the case of a perfect SC structure oriented in [0 0 1] and following the trivial path (no localization), the histogram would exhibit a bi-modal distribution. Two thirds of the elements are oriented perpendicular to the loading direction and carry nearly zero energy. The remaining 1/3 of the elements are aligned with the load. They share the energy evenly, resulting in a second peak in the histogram. Note that for this case the normalized energy is not changing with increasing overall deformation.

In contrast to the trivial solution, the consideration of the post-buckling path of the perfect structure gives rise to a different energy histogram (not shown, only discussed). After bifurcation a fraction of the elements experiences considerably higher energies. These values are isolated from the others and are rising with increas-

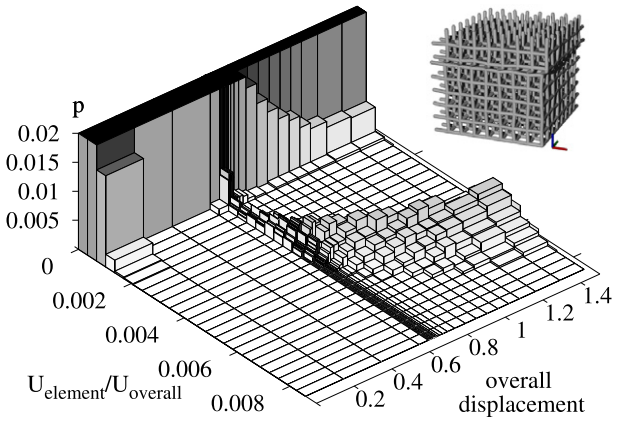


Fig. 8. Predicted energy distribution in the course of uniaxial vertical compression of a irregular ($\delta = l/16$) Simple Cubic finite structure with lattice orientation [0 0 1]; total energy within each Finite Element normalized by the overall work, $U_{\text{element}}/U_{\text{overall}}$, vs. fraction of elements, $p$ (cut off at $p = 0.02$).

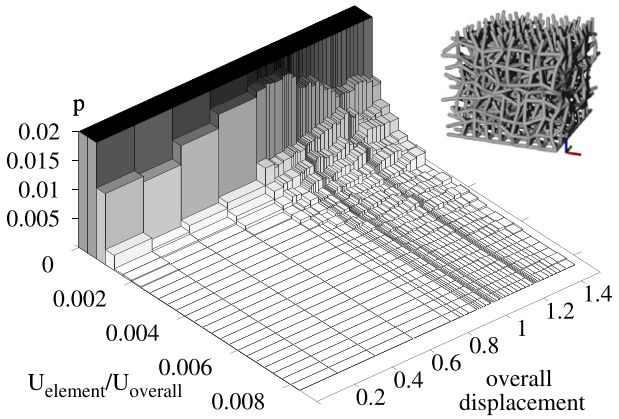


Fig. 9. Predicted energy distribution in the course of uniaxial vertical compression of a irregular ($\delta = 3l/8$) Simple Cubic finite structure with lattice orientation [0 0 1]; total energy within each Finite Element normalized by the overall work, $U_{\text{element}}/U_{\text{overall}}$, vs. fraction of elements, $p$ (cut off at $p = 0.02$).

ing overall deformation. In the present example this effect concerns about 1/8 of the load aligned elements. The energy distribution of the other elements is grossly unchanged.

Introduction of a small structural perturbation ($\delta = l/16$) yields the same appearance of the histogram as discussed before but with less pronounced peaks, Fig. 8. Increasing the structural perturbation results in a 'thicker' area of localization and being less pronounced. Consequently, the high energy peaks in the histograms move to lower values, become wider, and concern more elements. When the structural irregularities are large enough so that localization does not occur at all, the high energy peaks disappear completely. Their energy level is reduced until they are 'absorbed' in the low energy peaks, eventually. The latter, simultaneously, become more spread out as the irregularities increase. The resulting histogram is shown in Fig. 9 for the $\delta = 3l/8$ case.

Here, only the SC structure loaded in principal directions is discussed with respect to the effects of structural irregularities. These examples are considered as extreme cases showing all particular features, resembled to certain extents by all other cases.

## 4. Conclusions

The mechanical properties of porous open cell structures made from elastic–plastic bulk material are investigated by Finite Element simulations. Six regular three-dimensional generic structures are modeled by a unit cell approach and the entire elastic tensors are predicted. Out of this six, the Simple Cubic and the Kelvin type structures are studied further. Various degrees of structural irregularities are introduced while the density is kept constant and the effect on the elastic behavior is predicted. For the Simple Cubic structure the irregularities lead to a decrease of anisotropy. The Young's modulus in the principal structure direction is reduced, while in the other directions the stiffness increases. This means also that the stiffness sensitivity with respect to directions deviating from the principal directions is reduced. For the most irregular model investigated remarkable anisotropy is still left.

The Kelvin type structure shows the least elastic anisotropy among the regular geometries studied. Irregularities give rise to a moderate decrease of the Young's moduli in all directions. For the highest degree of perturbation cubic material symmetry is no longer obvious from the orientation dependent stiffnesses.

The nonlinear mechanical behavior of the Simple Cubic and the Kelvin structure is analyzed. The effect of structural irregularities on the localization of the deformation is studied under uniaxial compression. For large finite samples the overall stress–strain response is predicted for different lattice orientations. Histograms which show the statistical distribution of the total energy in the structures are introduced to assess the localization behavior.

For perfect and slightly irregular Simple Cubic type geometries a distinct localization is observed. The localization patterns are characteristics of the lattice inclination with respect to the loading direction. With increasing irregularities the localization areas become less "sharp". At the highest irregularities investigated localization is no longer occurring in Simple Cubic structures. For the selected lattice orientations an increase of the irregularities decreases the peak loads and gives rise to a smoother overall stress–strain behavior. This is most pronounced for loading parallel to the principal lattice orientation of the Simple Cubic structure.

The Kelvin structure does not exhibit a marked direction dependence in the nonlinear regime. Structural irregularities decrease the overall stress–strain response for all selected orientations. Localization is not found for the Kelvin type models. Introduction of irregularities change the Kelvin structures towards isotropic behavior with respect to elasticity and strength.

Structural irregularities have a marked effect for the Simple Cubic structures. The orientation dependence is decreased as well as the tendency to develop deformation localization. This is beneficial for energy absorption applications or when pronounced anisotropy and localization is considered detrimental. Kelvin structures, in general, are found to be close to isotropic. Irregularities do not change the behavior since the regular Kelvin structure already exhibits a quite complex geometry.

If the service load is known to be uniaxial compression of determined direction, Simple Cubic structures with irregularities may be advantageous. However, if a predominant loading direction is not known, Kelvin appears to be favorable. The peak load magnitude in the weakest direction for Simple Cubic is lower than for Kelvin.

Note that these conclusions are based on uni-axial compression load cases. For multi-axial loading scenarios additional simulations are likely to be required.

## Acknowledgement

This work was financially supported by the Austrian Science Fund under contract P15852.

## References

Anthoine, A., 1995. Derivation of the in-plane elastic characteristics of masonry through homogenization theory. International Journal of Solids and Structures 32 (2), 137–163.

Böhm, H.J., 2004. Mechanics of Microstructured MaterialsCISM Courses and Lectures, vol. 464. Springer-Verlag, Vienna (Ch. A short introduction to continuum micromechanics), pp. 1–40.

Christensen, R.M., 2000. Mechanics of cellular and other low-density materials. International Journal of Solids and Structures 37 (1–2), 93–104.

Daxner, T., 2003. Multi-scale modeling and simulation of metallic foams. Ph.D. Thesis, Vienna University of Technology, Vienna, Austria. Fortschritts-Berichte VDI, Reihe 18, No. 285. VDI Verlag, Düsseldorf.

Daxner, T., Böhm, H.J., Rammerstorfer, F.G., 1999. Influence of micro- and meso-topological properties on the crash-worthiness of aluminium foams. In: Banhart, J., Ashby, M.F., Fleck, N.A. (Eds.), Metal Foams and Porous Metal Structures. Verlag MIT, Bremen, pp. 283–288.

Daxner, T., Denzer, R., Böhm, H.J., Rammerstorfer, F.G., Maier, M., 2000. Simulation des elasto-plastischen Verhaltens von Metallschaum mit Hilfe von 2D und 3D Einheitszellen-Modellen. Materialwissenschaft und Werkstofftechnik 31, 447–450.

Duschlbauer, D., Böhm, H.J., Pettermann, H.E., 2006. Computational simulation of composites reinforced by planar random fibers: Homogenization and localization by unit cell and mean field approaches. Journal of Composite Materials, in press, doi:10.1177/0021998306062317.

Gan, Y.X., Chen, C., Shen, Y.P., 2005. Three-dimensional modeling of the mechanical property of linearly elastic open cell foams. International Journal of Solids and Structures 42 (26), 6628–6642.

Gibson, L.J., Ashby, M.F., 1988. Cellular Solids: Structure and Properties. Pergamon Press, Oxford, UK.

Gong, L., Kyriakides, S., 2005. Compressive response of open cell foams. Part II: Initiation and evolution of crushing. International Journal of Solids and Structures 42 (5–6), 1381–1399.

Gong, L., Kyriakides, S., Jang, W.-Y., 2005a. Compressive response of open-cell foams. Part I: Morphology and elastic properties. International Journal of Solids and Structures 42 (5–6), 1355–1379.

Gong, L., Kyriakides, S., Triantafyllidis, N., 2005b. On the stability of Kelvin cell foams under compressive loads. Journal of the Mechanics and Physics of Solids 53 (4), 771–794.

Grenestedt, J.L., 1999. Effective elastic behavior of some models for perfect cellular solids. International Journal of Solids and Structures 36 (10), 1471–1501.

Guo, X.E., Gibson, L.J., 1999. Behavior of intact and damaged honeycombs: a finite element study. International Journal of Mechanical Sciences 41 (1), 85–105.

Hohe, J., Becker, W., 2003. Geometrically nonlinear stress–strain behavior of hyperelastic solid foams. Computational Materials Science 28 (3–4), 443–453.

Kwon, Y.W., Cooke, R.E., Park, C., 2003. Representative unit-cell models for open-cell metal foams with or without elastic filler. Materials Science and Engineering A 343 (1–2), 63–70.

Li, K., Gao, X.-L., Subhash, G., 2005. Effects of cell shape and cell wall thickness variations on the elastic properties of two-dimensional cellular solids. International Journal of Solids and Structures 42 (5–6), 1777–1795.

Liska, R., Schwager, F., Woesz, A., Pisaipan, A., Seidler, S., Stampfl, J., 2003. A new route for the fabrication of biomimetic cellular materials. In: Proceedings Radtech 2003, Berlin. pp. 193–201.

Luxner, M.H., 2006. Modeling and simulation of highly porous open cell structures – elasto-plasticity and localization *versus* disorder and defects. Ph.D. thesis, Vienna University of Technology, Vienna, Austria.

Luxner, M.H., Stampfl, J., Pettermann, H.E., 2004. Linear and nonlinear numerical investigations of regular open cell structures. In: Proceedings of 2004 ASME International Mechanical Engineering Congress, Anaheim, USA, November 2004. ASME, New York.

Luxner, M.H., Stampfl, J., Pettermann, H.E., 2005. Finite element modeling concepts and linear analyses of 3D regular open cell structures. Journal of Materials Science 40 (22), 5859–5866.

Luxner, M.H., Stampfl, J., Woesz, A., Fratzl, P., Pettermann, H.E., 2006. Influence of structural disorder on the performance of 3D open cell structures. In: Proceedings of ECCM2006, Lisbon, Portugal. No. 1752.

Marsagli, G., 1972. Choosing a point from surface of a sphere. Annals of Mathematical Statistics 43 (2), 645–646.

Nye, J.F., 1985. Physical Properties of Crystals. Oxford University Press, Oxford, UK.

Pahr, D.H., 2003. Experimental and numerical investigations of perforated frp-laminates. Ph.D. thesis, Institute of Lightweight Structures and Aerospace Engineering, Vienna University of Technology.

Pettermann, H.E., Suresh, S., 2000. A comprehensive unit cell model: a study of coupled effects in piezoelectric 1–3 composites. International Journal of Solids and Structures 37 (39), 5447–5464.

Roberts, A.P., Garboczi, E.J., 2002. Elastic properties of model random three-dimensional open-cell solids. Journal of the Mechanics and Physics of Solids 50 (1), 33–55.

Shulmeister, V., Van der Burg, M.W.D., Van der Giessen, E., Marissen, R., 1998. A numerical study of large deformations of low-density elastomeric open-cell foams. Mechanics of Materials 30 (2), 125–140.

Silva, M.J., Gibson, L.J., 1997. The effects of non-periodic microstructure and defects on the compressive strength of two-dimensional cellular solids. International Journal of Mechanical Sciences 39 (5), 549–563.

Stampfl, J., Seyr, M.M., Luxner, M.H., Pettermann, H.E., Woesz, A., Fratzl, P., 2004. Regular, low density cellular structures – rapid prototyping, numerical simulation, mechanical testing. In: Aizenberg, J., Orme, C., Landis, W., Wang, R. (Eds.), Proceedings of 2004 MRS Spring Meeting – Biological and Bioinspired Materials and Devices. vol. 823, W8.8.

Woesz, A., Stampfl, J., Fratzl, P., 2004. Cellular solids beyond the apparent density–An experimental assessment of mechanical properties. Advanced Engineering Materials 6 (3), 134–138.

Zhu, H.X., Windle, A.H., 2002. Effects of cell irregularity on the high strain compression of open-cell foams. Acta Materialia 50 (5), 1041–1052.

Zhu, H.X., Knott, J.F., Mills, N.J., 1997. Analysis of the elastic properties of open-cell foams with tetrakaidecahedral cells. Journal of the Mechanics and Physics of Solids 45 (3), 319–325.

Zhu, H.X., Hobdell, J.R., Windle, A.H., 2000. Effects of cell irregularity on the elastic properties of open-cell foams. Acta Materialia 48 (20), 4893–4900.